Appl Phys A (2012) 108:911–920
DOI 10.1007/s00339-012-6993-4

Applied Physics A
Materials Science & Processing

Electrical conduction mechanism in nanocrystalline CdTe (nc-CdTe) thin films

Kriti Sharma · Alaa S. Al-Kabbi · G.S.S. Saini · S.K. Tripathi

Received: 8 November 2011 / Accepted: 10 May 2012 / Published online: 6 June 2012
© Springer-Verlag 2012

Abstract The present paper reports the electrical characterization of nc-CdTe thin films in different temperature ranges. Thin films of nc-CdTe are deposited on the glass substrates by Physical Vapor Deposition (PVD) using the Inert Gas Condensation (IGC) method. The Transmission Electron Microscopy (TEM) studies are made on the CdTe nanocrystals. The surface morphology and structure of the thin films are studied by the Scanning Electron Microscope (SEM) and X-Ray Diffraction (XRD) measurements. Dark conductivity measurements are made on the nc-CdTe thin films in the temperature range 110–370 K in order to identify the conduction mechanism in this temperature range. The obtained results reveal three distinct regions at high, low, and sufficiently low temperature regions with decreasing activation energies. The analysis of the high temperature conductivity data is based on the Seto's model of thermionic emission. At very low temperatures, dc conductivity (σ_d) obeys the law: $\ln \sigma T^{1/2} \propto T^{-1/4}$, indicating variable-range hopping in localized states near the Fermi level. The density of the localized states $N(E_F)$ and various other Mott's parameters like the degree of disorder (T_O), hopping distance (R), and hopping energy (W) near the Fermi level are calculated using dc conductivity measurements at low temperatures. Carrier type, carrier concentration, and mobility are determined from the Hall measurements. The transient photoconductivity decay measurements are performed on the nc-CdTe thin films at different intensities in order to know the nature of the decay process.

K. Sharma · A.S. Al-Kabbi · G.S.S. Saini · S.K. Tripathi (✉)
Centre of Advanced Study in Physics, Department of Physics, Panjab University, Chandigarh 160014, India
e-mail: surya@pu.ac.in
Fax: +91-172-2783336

S.K. Tripathi
e-mail: surya_tr@yahoo.com

1 Introduction

The investigation of the transport properties of II–VI compound semiconductor thin films, particularly CdSe, CdS, and CdTe have attracted considerable interest because of their high potential in photovoltaic devices. Thin films of these materials are used in many semiconductor devices such as photoconductors and photodetectors, IR detectors, solar cells, photodiodes, and field effect transistors [1, 2]. Most of the studies on thin films of these materials have concentrated on the electrical and optical properties.

Among these, CdTe is considered at present one of the most promising materials, for device applications. It has a high absorption coefficient in the visible range of the solar spectrum and its band gap is close to the optimum value for efficient solar energy conversion [2]. CdTe is unique among the semiconducting II–VI compounds, in its ability to exhibit both n-type and p-type conductivity at relatively high levels, which permits the utilization of solar cells in both homojunction and heterojunction configurations [3]. Considerable amount of data is available on the irradiation effects of γ-rays, electrons, and protons on CdTe films.

nc-CdTe thin films find its applications in the fabrication of cost effective thin film solar cells. The performance of such devices depends on the physical properties of the material, particularly in thin film form, which depends markedly on the preparation conditions. Different techniques of deposition have been developed to obtain device-grade CdTe thin films, among which electrodeposition [4], r.f. sputtering [5], closed space vapour transport [6], spray pyrolysis [7], and vacuum evaporation [8] are widely used. From the methods

discussed above, the thermal evaporation in vacuum using the Inert Gas Condensation (IGC) method is often preferred because it offers large possibilities to modify the deposition conditions and to obtain films with determined structure and properties. The IGC process is one of the most known and simple processes for the formation of nanoparticles. The structure of CdTe films is sensitive to preparation conditions and exists into two different types (Cubic zincblende and Hexagonal wurtzite structure). The performance and efficiency of thin film-based devices are determined strongly by the electrical, dielectric, and optical properties of the component films. A study of these properties and their dependence on the film properties is very important as it helps in optimizing film parameters for better device applications.

Al-Ghamdi et al. [9] and Shaaban et al. [10] have prepared nc-CdTe thin films by the thermal evaporation technique and investigated the effect of thickness on the optical properties of nc-CdTe thin films. Al-Ghamdi et al. [9] have found that the absorption coefficient, refractive index (n), and extinction coefficient (k) decrease while the values of the optical band gap increase with an increase in thickness. Singh et al. [11] have prepared nc-CdTe thin films by electrodeposition and determined their deposition potential, Cd:Te ratio, structural properties, morphological behavior, and the optical properties, respectively. Ikhmayies et al. [12] have studied the optical properties of nc-CdTe and calculated the effective band gap energies of the nanocrystallites. They have also estimated the radii of nanocrystallites using the hyperbolic band model. Nanocrystalline CdTe has been prepared by mechanical alloying using Cd and Te equiatomic powder mixture slight oxidized due to air exposition by Campos et al. [13]. The Raman results showed the disappearing of high frequency modes of α-TeO_2 after milling and suggested the photoinduced decomposition of CdTe phase. Changes of the physical and chemical properties of CdTe nanoparticles at increased temperature have been studied by thermal analysis and the probable mechanism has been proposed by Ban et al. [14]. Thus, from the above discussion, it is clear that considerable progress has been made in the understanding of the optical processes in nc-CdTe. Porter et al. [15] have measured the transport properties of CdTe NC films in FET structure. They have reported that majority carriers are holes and the hole density can be modulated with gate voltage. Variable range hopping conduction has also been studied in detail by some researchers. Mentzel et al. [16] have described the electrical transport properties of PbSe nanocrystals in FET structures by using a simple model of hopping between intrinsic localized states. Yu et al. [17] and Liu et al. [18] have studied variable range hopping conduction in nanocrystalline CdSe. There are only few reports which discuss the electrical conduction mechanism of nanocrystalline CdTe in different temperature ranges.

In the present work, the electrical properties of the nc-CdTe films in different temperature ranges have been investigated. nc-CdTe thin films are prepared by thermal evaporation using the IGC technique in the presence of argon as an inert gas. These thin films have been characterized using the Transmission Electron Microscopy (TEM) and X-Ray Diffraction (XRD) techniques. Electrical properties of these films have been studied in the different temperature ranges. In the low temperature region (110–160 K), the conduction has been found to exhibit a variable range hopping process while in the higher temperature region (>250 K), the thermionic emission of the carriers is responsible for the conduction over the grain boundaries. The electronic transport of the nc-CdTe thin films in the higher temperature range is explained using a model proposed by Seto [19]. Hall measurements are performed on the nc-CdTe thin films to calculate the carrier concentration, carrier type, and mobility of charge carriers.

2 Experimental

The CdTe material (99.999 % pure) used for the preparation of thin films has been purchased from Sigma–Aldrich. Thin films are prepared by thermal evaporation using the IGC technique in the presence of argon as inert gas at room temperature and on well-degassed Corning 7059 glass substrates. The material is evaporated from a heated Tungsten source into a chamber which has been previously evacuated to about 2×10^{-5} mbar. The films are kept in the deposition chamber in the dark for 24 hours before taking measurements to attain thermodynamic equilibrium. TEM has been done using the Hitachi H7500 electron microscope, operating at 100 kV. Samples for TEM measurements are prepared by depositing very thin layer of the material on carbon coated copper grids by thermal evaporation method using the IGC technique. The surface morphology of the nc-CdTe thin films on the glass substrate has been studied by using a Jeol Scanning Electron Microscope (JSM-6610 LV). Crystallographic study is carried out on the nc-CdTe in X-ray diffractometer (Spinner 3064 XPERT-PRO) using CuKα radiation in the 2θ range from 10° to 80°. The accelerating voltage is set at 45 kV with a current of 40 mA. The electrical measurements of these thin films are carried out in a specially designed metallic sample holder where heat filtered white light of the intensity 200 W tungsten lamp is shone through a transparent quartz window. A vacuum of 2×10^{-3} mbar is maintained throughout these measurements. Light intensity is measured using a digital luxmeter (MASTECH, MS6610). Planar geometry of the films (length ∼1.2 cm; electrode gap $\sim 8 \times 10^{-2}$ cm) is used for the electrical measurements. Thick Indium (In) electrodes used for electrical contacts are deposited by thermal evaporation at room temperature. For Hall measurements, four

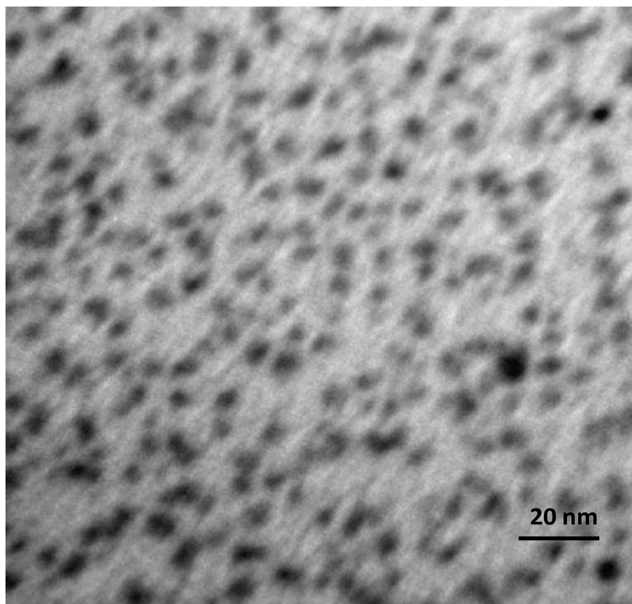

Fig. 1 TEM image of nanocrystals of CdTe

Indium electrodes are formed on the surface of nc-CdTe. Typical sample dimensions are ∼2.5 × 2.5 cm^2 and width of electrodes ∼1 mm^2. The photocurrent (I_{ph}) is obtained after subtracting the dark current (I_d) from the current measured in the presence of light. The dark and photocurrent are noted using a Keithley Electrometer (6517A).

3 Results and discussion

TEM image of the sample is shown in Fig. 1. The average size of the nanoparticles as obtained from the TEM is 3 nm. From the observed size of nanoparticles, it is difficult to say whether the majority of particles is in strong or weak confinement limit, which is defined by the exciton's Bohr radius, a_B being smaller (or larger) than the dimension of the spherical particle, respectively. Therefore, a_B is estimated for heavy-hole (hh) or light-hole (lh) excitons for CdTe using:

$$a_b = \left(\frac{4\pi\varepsilon_0\varepsilon_r\eta^2}{e^2\mu}\right) \quad (1)$$

where e is the elementary charge; ε_r, the static dielectric constant of the semiconductor ($\varepsilon_r = 10.2$) for CdTe [20] and $\mu = [m_e m_h/(m_e + m_h)]$ is the exciton's reduced mass, which depends on the effective masses, m_e of the electron and m_h of the hole. The effective mass of the hole can be approximated by m_{lh} for lh and m_{hh} for hh transitions. Using $m_e = 0.110m_0$, $m_{hh} = 0.600m_0$, and $m_{lh} = 0.180m_0$ [21] for CdTe, where m_0 is the free electron mass, results in $a_B^{lh} = 8$ nm for light hole, and $a_B^{hh} = 5$ nm for heavy hole excitons. The Bohr radii are more than the average particle size found in the TEM studies, i.e., $a_B \gg r$ which indicates the strong confinement in the CdTe nanoparticles.

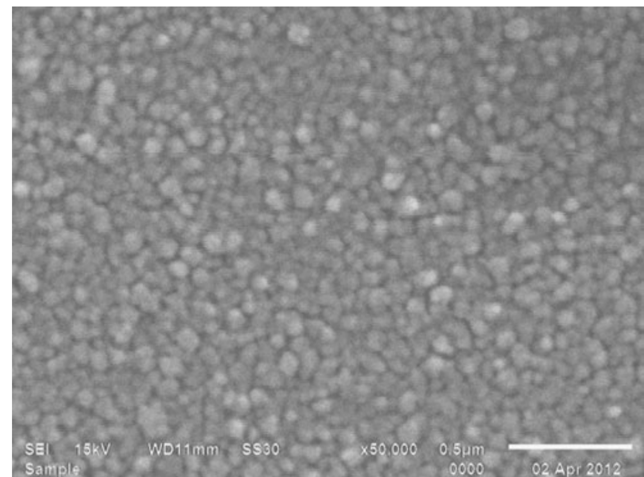

Fig. 2 SEM image of nc-CdTe thin film

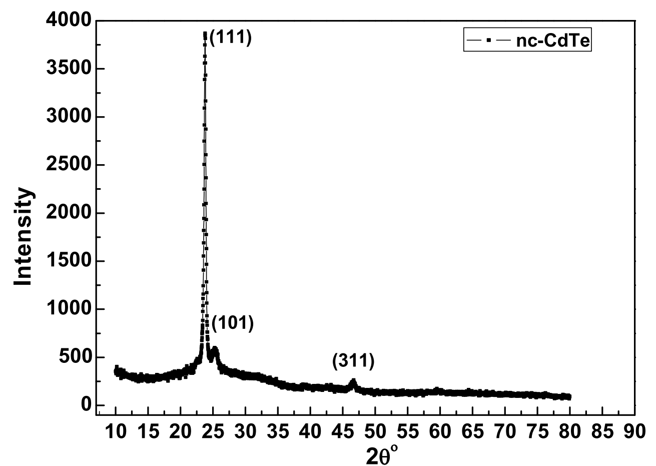

Fig. 3 XRD pattern of nc-CdTe thin film

Figure 2 shows the surface morphology of nc-CdTe thin film. The micrograph shows that the substrate is well covered with a large number of densely packed polycrystalline grains. The absence of cracks and pinholes in the micrograph reveals that the nc-CdTe thin films are smooth and have uniform surface.

Figure 3 shows the XRD pattern of nc-CdTe thin films. The corresponding peak positions and their calculated interplanar distance values d are listed in Table 1. The XRD pattern of the films show a mixed structure (cubic and hexagonal) with peaks at $2\theta = 23.8°, 25.8°$, and $46.5°$ corresponding to cubic (111), hexagonal (101) and cubic (311) orientations, respectively [22]. The intensity of the (111) peak is very strong, which confirms that the films have a preferential orientation of (111). Since the (111) direction is the close-packing direction of the zinc-blende structure and this type of ordering is often observed in polycrystalline films grown

Table 1 The calculated values of crystallite size (D), dislocation density (ε), strain (δ) for as- grown nc-CdTe thin films

Deposition condition	$2\theta°$	d (Å)	(hkl)	D (nm)	$\varepsilon \times 10^{-3}$ (lines^{-2} m^{-4})	$\delta \times 10^{15}$ (lines m^{-2})
As deposited	23.8°	3.74	(111)	26	1.37	1.48
	25.8°	3.52	(101)	10	3.48	10
	46.5°	1.95	(311)	12	2.81	6.94

on amorphous substrates [23]. Thus, nc-CdTe thin films are polycrystalline in the zinc-blende phase with (111) as the preferential orientation. The crystallite size (D) is calculated using the Scherrer formula [24] from the full-width at half-maximum (FWHM) (β) of the XRD peaks:

$$D = \frac{0.94\lambda}{\beta \cos\theta} \tag{2}$$

where λ is wavelength of the X-rays and θ is Bragg angle. The strain (ε) is calculated using the formula:

$$\varepsilon = \frac{\beta \cos\theta}{4} \tag{3}$$

The dislocation density (δ), defined as the length of dislocation lines per unit volume of the crystal, is evaluated from the formula [24]:

$$\delta = \frac{1}{D^2} \tag{4}$$

The average crystallite size of the nc-CdTe thin films is estimated to be 16 nm. The discrepancy between the particle size and crystallite size obtained from the TEM and XRD measurements may be due to the difference in the thickness of the samples studied for these measurements, since the TEM grid requires very thin layer deposition on the carbon coated copper grid. But for film characterizations (XRD, electrical characterization), film deposited on the glass substrate is thicker (several monolayers) as compared to that made for the TEM characterization.

Nanocrystalline thin films, in general, consist of grains and grain boundaries in the nanometer range and they are characterized by the presence of large surface to volume ratios of the crystallites constituting the film. This gives rise to properties different from those in the bulk in which there are large grains with a long range order. Grain boundaries play a significant role in the nanocrystalline materials because a large fraction of the atoms in the nanocrystalline materials is located within a few atomic distances of the grain boundaries. Understanding the origin of the unique properties of nanocrystalline materials requires complete study of the electrical conduction phenomena in different temperature ranges by using the existing theoretical models.

As observed from the SEM micrograph (Fig. 2), the conducting particles are in close proximity. So, electrons can jump gaps between the particles by tunnelling or hopping,

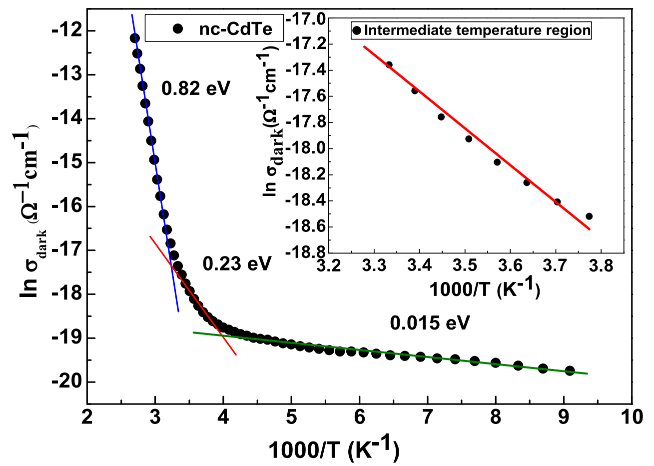

Fig. 4 Dependence of $\ln \sigma_d$ vs. $1000/T$ in the temperature range 110–370 K for nc-CdTe thin film. *Inset* shows variation of conductivity in intermediate temperature region

thus creating a current flow. Wuelfing et al. [25] have suggested an Arrhenius type activated tunnelling model to describe the transport phenomenon. The relation governing this phenomenon is given as

$$\sigma(x, T) = \sigma_0 . e^{-\beta x} . e^{\frac{-E_A}{kT}} \tag{5}$$

where β is the electron tunnelling coefficient, x is the average interparticle distance. The first term in the above expression gives the electron tunnelling between particles and depends exponentially on the distance. Thus, the probability of tunnelling decreases exponentially with interparticle distance [25].

The variation of the current with voltage is found to be linear up to the operating range of the applied voltage (graph not shown here) which shows the ohmic behavior. The temperature dependence of the dark conductivity (σ_d) of nc-CdTe thin films has been studied and ln σ_d vs. $1000/T$ curve is plotted in Fig. 4. On the basis of the nature of the slope, the temperature is divided into three regions [26] (high temperature region, intermediate temperature region, and low temperature region). The plot of $\ln \sigma_d$ vs. $1000/T$ in three temperature regions are straight lines, indicating that the conduction is through an activated process in all the three regions. The intermediate region is less clear and is shown in the inset of Fig. 4. The boundaries are approximate between regions where a particular conduction mechanism dominates. Furthermore, the passage from one region to another is not sharp; the straight lines in three temperature regions meet smoothly at the boundaries.

Low-temperature (100–160 K) data for these samples has been replotted as $\ln \sigma T^{1/2}$ vs. $T^{-1/4}$ (Fig. 5). According to Mott [27], the linear region of this plot represents an electron transport by hopping among localized states. The conductivity in the low-temperature region increases slowly with

Table 2 Electrical parameters of as-deposited nc-CdTe thin films

Sample	σ_d at 300 K (Ω^{-1} cm^{-1})	T_0 (K)	$N(E_f)$ (eV^{-1} cm^{-3})	R (cm)	W (eV)	αR
As deposited nc-CdTe	2.89×10^{-8}	1.81×10^5	2.20×10^{21}	1.81×10^{-7}	0.018	2.24

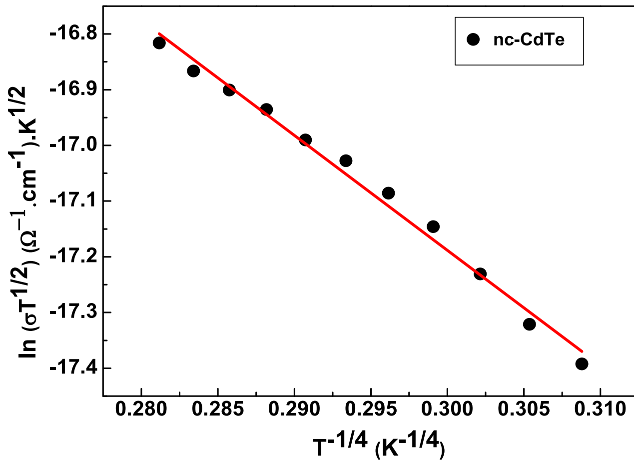

Fig. 5 The plot of $\ln \sigma T^{1/2}$ vs. $T^{-1/4}$ for nc-CdTe thin film

an increase in the temperature, which suggests that the conduction is due to the variable-range hopping in the localized states near the Fermi level. In amorphous materials, variable range hoping conduction (VRH) occurs at temperatures at which the phonons do not have sufficient energy for transfer to a nearest neighbor atom and charge carrier hops from a neutral atom to another neutral atom situated at the same energy level which can be situated at many interatomic distances away. However, in polycrystalline materials, the VRH conduction process exists in the grain boundaries at temperatures at which the carriers do not have sufficient energy to cross the potential barrier and to transfer themselves into grain by the process of thermionic emission. However, hopping in this case takes place due to the transfer of the charge carriers from a charged trap state to a neutral trap state [28].

This variable-range hopping (VRH) mechanism is characterized by Mott's [29–31] expression:

$$\sigma_d T^{1/2} = \sigma_0 \exp\left(-\left(\frac{T_0}{T}\right)\right)^{\frac{1}{4}} \tag{6}$$

The preexponential factor (σ_0) and the degree of disorder (Mott temperature) T_0 are related to the density of states $N(E_F)$, and the inverse-fall-off length of the wave function of a localized state near the Fermi-level α by the following relations [32]:

$$\sigma_0 = \frac{3e^3 \upsilon_{ph}}{(8\pi k)^{\frac{1}{2}}}\left[\frac{N(E_F)}{\alpha}\right]^{\frac{1}{2}}, \tag{7}$$

$$T_0 = C_0 \frac{\alpha^3}{kN(E_F)} \tag{8}$$

where $N(E_F)$ is the density of hopping sites at the Fermi level and $C_0 = 18$ is a numerical constant which depends on the detailed assumptions. α is the coefficient of the exponential decay of the localized states wave function and is assumed to be 0.124 Å^{-1} [33–35]. The experimental data obey Mott's VRH relation [36], giving rise to a linear relationship between $\ln(\sigma T^{1/2})$ and ($T^{-1/4}$) as is clear from Fig. 5. Therefore, the conduction mechanism at low temperature is due to the hopping of the charge carriers among the localized states. Other Mott parameters, the distance R, and average energy W are determined at $T = 140$ K using the following relations [31]:

$$R = \left[\frac{9}{8\pi\alpha kTN(E_F)}\right]^{\frac{1}{4}}, \tag{9}$$

$$W = \frac{3}{4}\pi R^3 N(E_F) \tag{10}$$

From the slope of Fig. 5, we have calculated various Mott parameters such as the degree of disorder (T_0), density of states ($N(E_F)$), hopping distance (R), and hopping energy (W) for nc-CdTe thin films at 140 K as listed in Table 2. According to Mott and Davis [37–41], αR and W should have values greater than unity and kT, respectively, for VRH conduction. It is evident from this Table 2, $\alpha R > 1$ and $W > kT$, which agrees with the Mott's condition for VRH. Degree of localization of the carriers in the trap states, indicated by $\alpha R > 1$, shows that the charges are highly localized. From the above discussion, it may be concluded that at low temperatures, σ obeys the law: $\ln \sigma T^{1/2} \propto T^{-1/4}$, indicating VRH in localized states near the Fermi level [42].

In the temperature range (255–370 K), the plots of $\ln \sigma_d$ vs. $1000/T$ have two linear portions, first in the lower temperature range (255–310 K), characterized by a small slope and second in the high temperature range (315–370 K), characterized by large slope. The electronic transport properties of thin polycrystalline semiconductor films are strongly influenced by their structural characteristics (the crystallite shape and size, intercrystal boundaries, lattice defects, etc.) and purity (nature and concentration of the impurities, adsorbed and absorbed gases, etc.). So, the conduction mechanism in nc-CdTe thin film samples can be explained on the basis of the models [43, 44] developed for the films with polycrystalline (discrete) structure. These models are based upon the consideration that the crystallite boundaries have a space charge region due to the interface [43, 44]. The Seto's

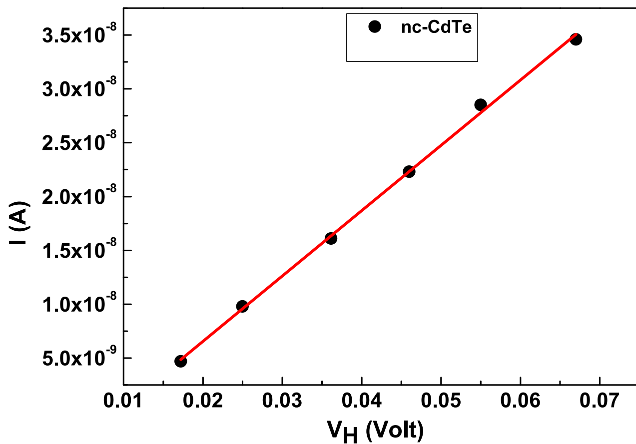

Fig. 6 The plot of Hall Voltage (V_H) vs. current (I) for nc-CdTe thin films

model [19, 45] with several modifications proposed by Baccarani et al. [46, 47] could explain the mechanism of electron transfer in nc-CdTe films. The following assumptions have been made in this model: (i) the crystallites have similar size and shape, (ii) only one type of monovalent trapping states (having concentration N_t and energy E_t with respect to Fermi level at the interface E_i) is present and is uniformly distributed within crystallites, (iii) the traps are initially neutral and become charged by trapping a free carrier and (iv) the crystallite boundary thickness is negligible with respect to crystallite size.

The Hall measurements have been used to investigate the type and concentration of charge carriers. Figure 6 shows the variation of current (I) vs. Hall voltage (V_H) for nc-CdTe film. Using the slope of this curve, we have found carrier concentration. The results of the Hall measurements indicate that the nc-CdTe film has p type conduction with carrier density $1.13 \times 10^{13}/\text{cm}^3$. The hole mobility for nc-CdTe is about 1.59×10^{-2} $\text{cm}^2/\text{V}\cdot\text{sec}$ which is small. The major reason for small mobility may be due to the scattering of carriers at grain boundaries, since the grain size of nc-CdTe is as small as 16 nm. The obtained results are in accordance with the results obtained by M. Miyake et al. [48].

Since the CdTe crystallites' are p type as confirmed by Hall measurements and N_A is defined as the acceptor concentration. For any assigned values of L, N_t, and E_t, there will be an impurity concentration N_A^* such that, when $N_A < N_A^*$ the crystallites are entirely depleted and the energy barrier can be written in the form [46]:

$$E_b = \frac{e^2 D^2 N_A}{8\varepsilon_r} \tag{11}$$

and in this case electrical conductivity of thin films can be expressed as

$$\sigma_f = e^2 D^2 N_C N_A \nu \left[2kT(N_t - DN_A)\right]^{-1} \exp\left(\frac{-E_a}{KT}\right) \tag{12}$$

where

$$\nu = \left(\frac{kT}{2\pi m^*}\right)^{\frac{1}{2}} \tag{13}$$

and activation energy is given by

$$E_a = \frac{1}{2}E_g - E_t \tag{14}$$

In the second case, $N_A > N_A^*$, the crystallites are partially depleted and the expression of electrical conductivity can be determined corresponding to the two following energy domains [47]:

- For energy domain

$$E_f - E_t - E_b \gg kT \tag{15}$$

Electrical conductivity of the film can be described by the expression

$$\sigma_f = \frac{e^2 D N_C^2 \nu n_o}{kT} \exp\left(\frac{-E_a}{kT}\right) \tag{16}$$

and the activation energy E_a is

$$E_a = E_b \tag{17}$$

- For energy domain

$$E_t + E_b - E_f \gg kT \tag{18}$$

Electrical conductivity of the films can be written as

$$\sigma_f = eN_C^2\left(2\varepsilon_r N_A^{-1} E_b\right)^{\frac{1}{2}} (kTN_t)^{-1} \exp\left(\frac{-E_a}{kT}\right) \tag{19}$$

where

$$E_a = \frac{1}{2}E_g - E_t \tag{20}$$

In the Eqs. (11)–(20), the following notations have been used: e, electron charge; D, average size of the crystallites; N_C, effective state density for the conduction band; k, Boltzmann's constant; N_t, concentration of surface (interface) states with E_t energy with respect to E_i at the interface; T, absolute temperature; m^*, scalar effective mass of charge carriers; E_g, energy bandgap (forbidden band); E_b, barrier height (crystallite boundary, barrier potential); ε_r, low-frequency dielectric constant of crystallites; no, electron concentration in neutral region of crystallites, and E_F, energy of Fermi level.

By assuming that in the lower temperature range ($255\ \text{K} < T < 285\ \text{K}$), the expression (16) is valid. From the slopes of $\ln\sigma$ vs. $10^3/T$ curves in this temperature range, the values of the energy barrier, E_b, have been calculated. These values are listed in Table 3. The values of impurity concentrations N_A, have been calculated by taking into account the expression (11). In this expression, the values of the crystallite size have been determined by XRD and the low frequency dielectric constant is taken to be 10.2 [20]. The obtained values for N_A are also indicated in Table 3.

Table 3 Characteristic parameters of investigated sample* using Seto model

Sample	D (nm)	ΔT_t (K)	E_b (eV)	E_{a1} (eV)	E_{a2} (eV)	T_1 (K)	T_2 (K)	T_3 (K)	N_A (cm^{-3})	N_t (cm^{-2})
nc-CdTe	16	255–370	0.16	0.23	0.82	255	310	370	3.54×10^{19}	5.67×10^{13}

$^*D$, average size of crystallites; ΔT_t, temperature range in which sample is given heat treatment; E_b, barrier height, E_{a1}, activation energy for the temperature range $\Delta T = T_2 - T_1$; E_{a2}, activation energy for the temperature range $\Delta T = T_3 - T_2$; N_A, impurity concentration; N_t, concentration of surface states

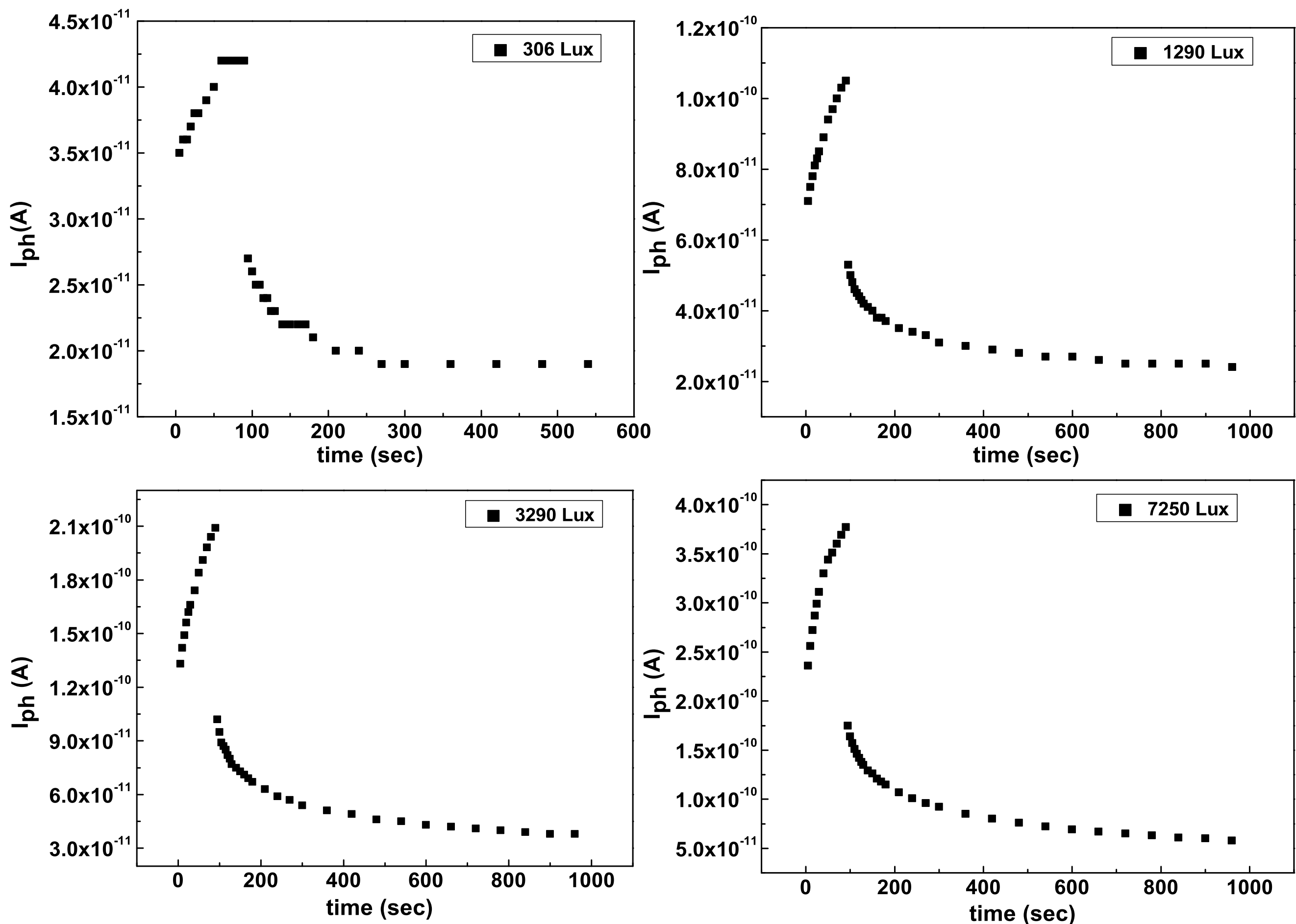

Fig. 7 Rise and decay of photocurrent at different intensities for nc-CdTe thin films

Substituting the N_A and σ_f values at 365 K into Eq. (12) (the values of σ_f have been estimated from the $\ln\sigma$ vs. $10^3/T$ curves), the values of N_t are calculated which are also listed in Table 3. For the investigated sample, the value of scalar effective mass of charge carriers is assumed to be $m^* = 0.35$ m_o (m_o is free electron mass) [20].

The study of transient photoconductivity measurements as a function of light intensity is a valuable tool in achieving a good understanding of the recombination process and distribution of localized states which control the phototransport kinetics. In order to understand the recombination and trapping mechanisms, transient photoconductivity measurements are conducted by exposing the sample at different light intensities at 300 K. Figure 7 shows the rise and decay of photocurrent in nc-CdTe film at different intensities. It is evident from the figure that the photocurrent rises in a monotonic manner. After cessation of steady illumination, trapped electrons and holes combine and the photocurrent decay is initially quite fast and then reaches a steady-state value known as the persistent photocurrent. This persistent photocurrent may not be simply due to carriers trapped in the localized states. So, to simplify the analysis, the persistent photocurrent is subtracted from the measured photocurrent.

The decay of the photocurrent is plotted at different intensities on a semilogarithmic scale as shown in Fig. 8. These

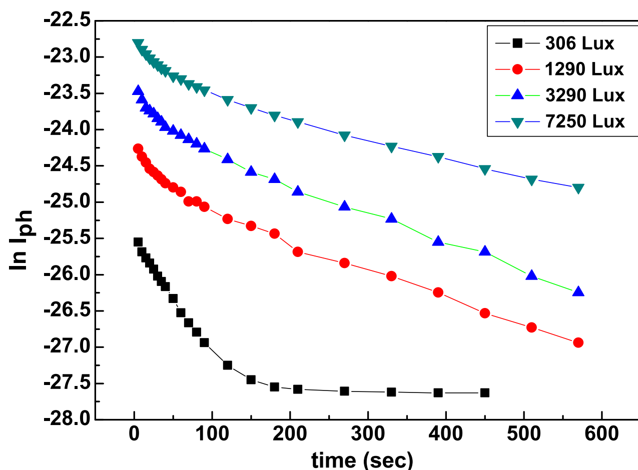

Fig. 8 Plot showing variation of $\ln I_{ph}$ vs. time (t) at different intensities

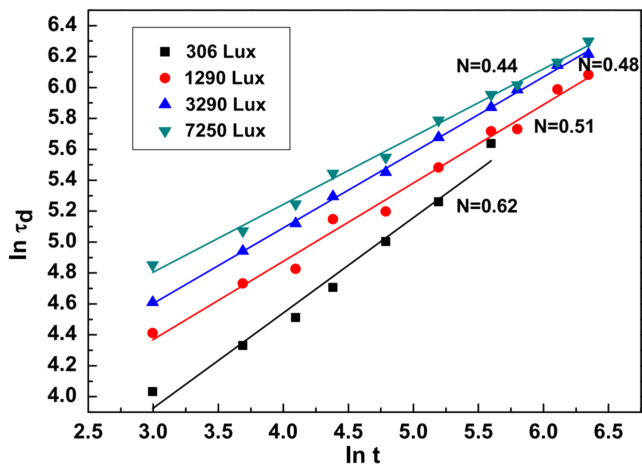

Fig. 9 Plot of $\ln \tau_d$ vs. $\ln t$ for nc-CdTe thin films at different intensities

curves must be straight lines in case of a single trap level. But Fig. 8 shows that $\ln I_{ph}$ vs. t curves are not straight lines. Also, the slope of the decay curve goes on decreasing continuously as the time of decay increases. This indicates that the traps may be present at all the energies in the bandgap of sample. These traps have different time constants, and hence give the nonexponential decay of photoconductivity. To analyze the decay rates in the case of nonexponential decay, the differential lifetime (τ_d) is calculated using the relation [49]:

$$\tau_d = -\left[\frac{1}{I_{ph}}\left(\frac{dI_{ph}}{dt}\right)\right]^{-1} \tag{21}$$

From the slopes of the I_{ph} vs. time curves, we have calculated the values of τ_d using Eq. (21) at various times of the decay curve of Fig. 7. The decay times observed for nc-CdTe thin films at all intensities are found to be time dependent. In order to study the dependence of τ_d with time, τ_d is plotted against t on a double logarithmic scale at different intensities as shown in Fig. 9. The plots are found to be straight lines indicating that the decay is time dependent and nonexponential [50]. If the decay is nonexponential, then the decay law is hyperbolic, and obeys the power law of the form t^{-n} [50, 51]

$$n = \frac{d(\ln \tau_d)}{d(\ln t)} \tag{22}$$

If the value of n is unity, the distribution of traps is uniform, otherwise it is said to be nonuniform or quasiuniform. In the present case, values of n vary in the range of 0.44–0.62, which shows the distribution of traps is nonuniform. Also, from Fig. 9, the values of τ_d increase with an increase in the intensity of light which may be due to increase in trap levels induced by light.

Transient conductivity also provides information of some other processes such as dispersive transport. Nonexponential decays arise from the thermal excitation of electrons from the traps when there is a distribution of traps; in particular, a power-law decay results when the distribution is exponential in energy $N(E)$ of the form [52]:

$$N(E) = \left(\frac{N_t}{E_O}\right)\exp\left(\frac{-E}{E_O}\right) \tag{23}$$

where N_t is the total gap state density and $E_O = kT_O$ is the distribution parameter.

According to the trap controlled recombination model [53], the photocurrent decay depends on the initial density of photogeneration pulse when the total filling of gap states is not achieved. Thereafter, an initial portion of the decay is governed by the capture process and the recombination is delayed. Over this portion, $I_{ph} \sim I_O t^{-1(1-\alpha)}$, where I_O is the photocurrent at the moment when the light is switched off and α is the dispersion parameter. The dispersion parameter α is determined from the experimental relaxation curves as an asymptotic of the power-law portions of decay photocurrent, i.e., $\ln I_{ph}$ vs. $\ln t$ plot (graph not shown) of nc-CdTe thin films at different intensities. The localized state distribution parameter E_O is also estimated using the values of the dispersion parameter α, using the relation $\alpha = kT/E_O$, where k is Boltzmann's constant and T is the ambient temperature. Now $E_O = kT_O$ is the characteristic energy of the density of state distribution and T_O is the characteristic temperature. T_O [54] is defined as the temperature at which the impurities or the fluctuations of the potentials are frozen in the cooling process. Also, T_O determined for various impurities also reflects the temperature for which the diffusion coefficient of the impurities becomes negligibly small [55]. Thus, α and relative parameters are determined from the slope of $\ln I_{ph}$ and $\ln t$ (not shown) and are tabulated in Table 4. The similar type of behavior has been reported by our group on GeSeCu thin films [56].

Table 4 Parameters α, E_O, and T_O for nc-CdTe thin films

nc-CdTe	α	E_O (eV)	T_O (K)
306 Lux	0.66	0.039	453
1290 Lux	0.72	0.036	419
3290 Lux	0.73	0.035	407
7250 Lux	0.77	0.033	384

In our study, we have tried to make a special effort in understanding the charge carrier transport properties of nc-CdTe thin films due to its potentially economic applications in solar cells and other optoelectronic devices. The electrical transport properties of the materials are of great importance in determining whether the material is congruent with our necessities or not. We have studied the temperature dependence of electrical conductivity of nc-CdTe thin film which offers a lot of information on the electrical conduction mechanism in the respective films in correlation with their structure. In semiconducting thin films, carrier transport may be influenced by the presence of native defects, various trapping levels defect impurity complexes, and self diffusion processes [57]. These trapping levels are the centers of preferential recombination and one of the main causes of the small minority carrier lifetimes which is the main cause of poor luminescence. We have chosen nc-CdTe system for study because for this system (in the temperature ranges under study) the native defects only play a secondary role in terms of complex formation with impurities [57]. We have calculated the concentration of impurity atoms (N_A) and various trap states (N_t) in nc-CdTe thin films using the Seto model. It can be observed that the values obtained for N_t are equal with common values of this parameter calculated for different II–VI semiconducting compounds (CdS, CdSe, ZnSe) in thin film form [43].

4 Conclusions

Electrical conduction mechanism of the nc-CdTe thin films is investigated in the temperature range 110–370 K. It has been observed that the conduction at low temperatures takes place through a variable range hopping of charge carriers in the localized states near the Fermi level (E_F), which is in fair agreement with the Mott's condition of variable range hopping conduction. The density of the localized states is calculated using Mott's parameters. nc-CdTe thin films are found to be p type from Hall measurements. Carrier concentration (p) and Hall mobility (μ_H) are also calculated. The high temperature data on the other hand has been explained on the basis of Seto's model for thermionic emission of the carriers over the grain boundaries in nc-CdTe. The results of transient photoconductivity measurements show that the decay is time dependent and nonexponential. The dispersion parameter (α) of the localized state energy distribution, determined from the decay curves at different intensities is also calculated.

Acknowledgements This work is financially supported by the Department of Science and Technology (Major Research Project), N. Delhi. Ms. Kriti Sharma is thankful to UGC, N. Delhi for providing the fellowship.

References

1. S.K. Tripathi, J. Mater. Sci. **45**, 5468 (2010)
2. O. Koudriavtseva, A. Morales-Acevedo, Yu. Kudriavtsev, S. Gallardo, R. Asomoza, R. Mendoza-Perez, J. Sastre-Hernandez, G. Contreras-Puente, Appl. Surf. Sci. **255**, 1423 (2008)
3. E. Matei, L. Ion, S. Antohe, R. Neumann, I. Encutescu, Nanotechnology **21**, 105202 (2010)
4. S. Ham, B. Choi, N. Myung, N.R. de Tacconi, C.R. Chenthamarakshan, K. Rajeshwar, Y. Son, J. Electroanal. Chem. **601**, 77 (2007)
5. Y.-O. Choi, N.-H. Kim, J.-S. Park, W.-S. Lee, Mater. Sci. Eng. B **171**, 73 (2010)
6. J. Aguilar-Hernández, G. Contreras-Puente, J. Vidal-Larramendi, O. Vigil-Galán, Thin Solid Films **426**, 132 (2003)
7. V.V. Ison, A. RangaRao, V. Dutta, Sol. Energy Mater. Sol. Cells **93**, 1507 (2009)
8. Y. Sato, H. Hatori, S. Igarashi, M. Arai, K. Ito, S. Kikuchi, Curr. Appl. Phys. **10**, S499 (2010)
9. A.A. Al-Ghamdi, S.A. Khan, A. Nagat, M.S. Abd El-Sadek, Opt. Laser Technol. **42**, 1181 (2010)
10. E.R. Shaaban, N. Afify, A. El-Taher, J. Alloys Compd. **482**, 400 (2009)
11. R. Raj Singh, D. Painuly, R.K. Pandey, Mater. Chem. Phys. **116**, 261 (2009)
12. S.J. Ikhmayies, R.N. Ahmad-Bitar, Physica B **405**, 3141 (2010)
13. C.E.M. Campos, K. Ersching, J.C. de Lima, T.A. Grandi, H. Höhn, P.S. Pizani, J. Alloys Compd. **466**, 80 (2008)
14. I. Ban, M. Kristl, V. Danč, A. Danč, M. Drofenik, Mater. Lett. **67**, 56 (2012)
15. V.J. Porter, T. Mentzel, S. Charpentier, M.A. Kastner, M.G. Bawendi, Phys. Rev. B **73**, 155303 (2006)
16. T.S. Mentzel, V.J. Porter, S. Geyer, K. MacLean, M.G. Bawendi, M.A. Kastner, Phys. Rev. B **77**, 075316 (2008)
17. D. Yu, C. Wang, B.L. Wehrenberg, P.G. Sionnest, Phys. Rev. Lett. **92**, 216802-1 (2004)
18. H. Liu, A. Pourret, P.G. Sionnest, ACS Nano **4**, 5211 (2010)
19. J.Y.W. Seto, J. Electrochem. Soc. **122**, 701 (1975)
20. G.P. Kissling, D.J. Fermin, Phys. Chem. Chem. Phys. **11**, 10080 (2009)
21. F. Long, W.E. Hagston, P. Harrison, T. Stirner, J. Appl. Phys. **82**, 3414 (1997)
22. S. Lalitha, R. Sathyamoorthy, S. Senthilarasu, A. Subbarayan, Sol. Energy Mater. Sol. Cells **90**, 694 (2006)
23. A.L. Dawar, K.V. Ferdinand, C. Jagdish, P. Kumar, P.C. Mathur, J. Phys. D, Appl. Phys. **16**, 2349 (1983)
24. G. Shanmugavelayutham, V. Selvarajan, Bull. Mater. Sci. **27**, 453 (2004)
25. W.P. Wuelfing, R.W. Murray, J. Phys. Chem. B **106**, 3139 (2002)
26. Y. Yao, C. Liu, H. Qi, X. Chang, C. Wang, G. Wang, Curr. Appl. Phys. **11**, 620 (2011)
27. N.F. Mott, Philos. Mag. **19**, 835 (1969)
28. A.A. Abu-Sehly, M.I. Abd-Elrahman, J. Phys. Chem. Solids **63**, 163 (2002)

29. A. Rockett, *The Materials Science of Semiconductors* (Springer, New York, 2007)
30. M.L. Theye, in *Proceedings of the Fifth International Conference on Amorphous and Liquid Semi-conductors*, vol. 1, Garmisch-Partenkirchen, Germany (1973)
31. N.F. Mott, E.A. Davis, *Electronic Processes in Non-crystalline Materials* (Clarendon Press, Oxford, 1970)
32. N.F. Mott, E.A. Davis, *Electronic Processes in Non-Crystalline Materials*, 2nd edn. (Clarendon Press, Oxford, 1979)
33. S. Ramchandar Rao, M. Nagabhooshanam, V. Hari Babu, Cryst. Res. Technol. **25**, 55 (2006)
34. M. Thamilselvan, K. Premnazeer, D. Mangalaraj, Sa.K. Narayandass, J. Yi, Cryst. Res. Technol. **39**, 137 (2004)
35. C.H. Seager, G.E. Pike, Phys. Rev. B **10**, 1435 (1974)
36. A.F. Qasrawi, M.M. Shukri Ahmed, Cryst. Res. Technol. **41**, 364 (2006)
37. T.G. Abdel-Malik, R.M. Abdel-Latif, A. Sawaby, S.M. Ahmed, J. Appl. Sci. Res. **4**, 331 (2008)
38. V.A. Twaddell, W.C. Lacourse, J.D. Mackenzie, J. Non-Cryst. Solids **8**, 831 (1972)
39. A.F. Qasrawi, M.M. Shukri Ahmed, Cryst. Res. Technol. **41**, 364 (2006)
40. J.M. Marshall, C. Main, J. Phys. Condens. Matter **20**, 285210 (2008)
41. N.F. Mott, E.A. Davis, Philos. Mag. **22**, 903 (1970)
42. C. Viswanathan, G.G. Rusu, D. Mangalaraj, Sa.K. Narayandass, J. Yi, J. Optoelectron. Adv. Mater. **7**, 713 (2005)
43. G. Harbeke (ed.), *Polycrystalline Semiconductors: Physical Properties and Applications* (Springer, Berlin, 1985)
44. L.L. Kazmerski (ed.), *Polycrystalline and Amorphous Thin Films and Devices* (Academic Press, New York, 1980)
45. J.Y.W. Seto, J. Appl. Phys. **46**, 5247 (1975)
46. G. Baccarani, B. Ricco, G. Spandini, J. Appl. Phys. **49**, 5565 (1978)
47. C.H. Seager, T.G. Gastner, J. Appl. Phys. **49**, 3879 (1978)
48. M. Miyake, K. Murase, T. Hirato, Y. Awakura, J. Electrochem. Soc. **150**, C413 (2003)
49. W. Fuhs, D. Meyer, Phys. Status Solidi A **24**, 275 (1974)
50. D.P. Padiyan, A. Marikani, K.R. Murali, Mater. Chem. Phys. **78**, 51 (2002)
51. R. Sathyamoorthy, P. Sudhagar, C. Chandramohan, K.P. Vijya Kumar, Cryst. Res. Technol. **42**, 498 (2007)
52. I. Sharma, A. Kumar, S.K. Tripathi, P.B. Barman, J. Phys. D, Appl. Phys. **41**, 175504 (2008)
53. M.S. Ivou, S.D. Shutov, V.I. Arkhipov, G.I. Adriaensens, J. Non-Cryst. Solids **299**, 1008 (2002)
54. V. Vaninov, J. Orenstein, M.A. Kastner, Philos. Mag., B **45**, 399 (1982)
55. M.A. Kastner, Philos. Mag., B **37**, 127 (1978)
56. A. Thakur, V. Sharma, G.S.S. Saini, N. Goyal, S.K. Tripathi, J. Phys. D, Appl. Phys. **38**, 2005 (1959)
57. R. Bhargava (ed.), *Properties of Wide Bandgap II–VI Semiconductors* (Inspection, London, 1997)